Zero-Sequence Voltage Elimination for Dual Fed Common dc-link Open-End Winding PMSM High Speed Starter-Generator, Part I: Modulation

Luca Rovere, *Member, IEEE,* Andrea Formentini, *Member, IEEE,* Giovanni Lo Calzo, Pericle Zanchetta, *Senior Member, IEEE* Tom Cox, *Member, IEEE,*

Abstract—In this paper a dual-fed common dc-link topology Open-End Winding Permanent Magnet Synchronous Motor (OEW-PMSM) for aircraft high speed Starter-Generator application is considered. While on one hand the common dc bus configuration significantly simplifies and reduces the costs of the topology, on the other hand it allows the Zero-Sequence Current (ZSC) to flow freely in the system. High speed machines are characterized by low phase inductance which implies low Zero-Sequence Impedance (ZSI). A small time constant of the zero-sequence circuit produces a high frequency, high intensity ZSC ripple with the risk of harming the switching devices. This paper presents a novel hybrid Space Vector Pulse Width Modulation (SVPWM) that allows to instantaneously eliminate the Zero-Sequence Voltage (ZSV) produced by the two Voltage Source Converters (VSCs) by square wave modulating one of the two VSCs. The non-sinusoidal machine back Electro Magnetic Force (back EMF) has been considered and the effect of the converters' Dead Time (DT) on the ZSV has been analysed. The square wave modulated VSC uses IGBT devices while the other uses SiC technology. The proposed topology is tested through both simulations and experiments.

Index Terms—Open-End Winding Machine, Permanent Magnet Synchronous Motor, Dual-Fed Single dc-link drive, Dead-Time, Zero-Sequence Voltage, Zero-Sequence Current.

I. INTRODUCTION

The advantages of the OEW configuration for ac machines drives were already investigated in [1] showing how three-level inversion could be realized with two two-level inverters connected at each end of the machine. Furthermore the dual-fed OEW topology allows for increased fault-tolerant capability [2], [3], reduction of the dc-link voltage by half and redundant space-vector combinations. The dual-fed OEW configuration has found a wide range of applications such as wind power generation [4], [5], electric vehicles [6], [7], high power electric propulsion [8] and aircraft starter-generator systems [9]–[11]. Two isolated dc power supplies [12], one dc supply and a floating bridge [13] or a single dc supply [14] can be adopted for the dual-fed OEW. While on one hand the common dc bus configuration significantly simplifies and reduces the costs of the topology, on the other hand it allows the ZSC to flow freely in the system. As widely discussed in [4], [15] the causes of a circulating ZSC can be attributed to ZSV generated by the converters, third harmonic component of the back EMF, devices' DTs, device's voltage drops and coupling between the dq axes and the 0-axis when the machine second harmonics of the self and mutual inductance are not the same [16]. The magnitude of the ZSC depends on the equivalent ZSI which
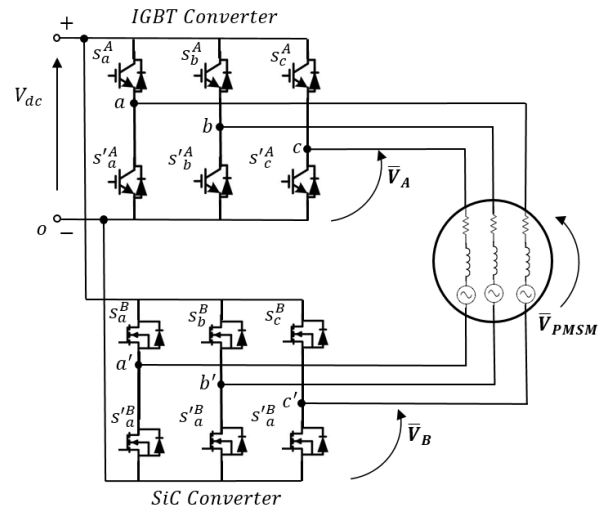

Fig. 1. Dual-Fed single dc-link OEW-PMSM with mixed technology VSCs.

is generally low as reported in [17], [18].With a particularly low phase inductance, and consequently even smaller ZSI the equivalent zero sequence circuit is less able to filter out the high-frequency components of the switched voltage. In other words, a small time constant of the zero-sequence circuit produces a high frequency, high intensity current ripple with the risk of harming the switching devices. In this work an high speed machine characterized by a low phase inductance of $355\mu H$ is considered, which is significantly lower than the one considered in previous papers [19] [4] [20](respectively $8.5mH$, $61.7mH$ and $17mH$).

The more the machine inductance is low the more problems associated with the circulation of a ZSC are going to be enhanced leading to high intensity ZSC ripple. The ZSC reduces the overall system efficiency therefore many works focused on VSCs' modulations to reduce or eliminate the zero-sequence component of the voltage supplied to the machine. In [17] a SVM that aims to set to zero the average ZSV produced by the two VSCs by zero vector time redistribution is proposed for an induction motor drive. In [19] a PMSM with perfectly sinusoidal back EMF is considered and a SVM where the average ZSV applied by the converters is zero is developed. In [16] a modulation which allows to provide a controllable ZSV component in order to synthesize the zero-sequence controller output is proposed. Many works introduce

modulations which allow to synthesize a reference ZSV in order to implement controllers that would allow to eliminate the ZSC flowing due to the machine's non-sinusoidal back-EMF. In [19] a PI regulator for the zero-axis in combination with a SVM where the average ZSV applied by the converters is zero is proposed. In order to better eliminate the sinusoidal ZSC a Proportional Resonant (PR) controller is implemented in [4], where the reference ZSV is synthesized by zero vector redistribution. Similarly, in [16] a frequency adaptive PR controller is used since the ZSC frequency changes according to the operating speed. In this paper a dual-fed common dc-link topology OEW-PMSM for aircraft high speed Starter-Generator application is considered. SiC technology in combination with standard IGBT devices can be used to increase the system efficiency and drive the high speed machine as demonstrated in [10], [11]. The SiC devices can work at higher frequencies than the conventional IGBT with less switching losses. In this paper a modulation for the mixed technology dual-inverter is developed in order to exploit the different nature of the power devices and reduce the circulating ZSC. The focus of this work is to develop a modulation for the two VSCs that would allow to simultaneously exploit the different technologies and to eliminate the ZSV. Compared with previous works [16], [17], [19], the significantly lower ZSI does not allow to apply any ZSV. Therefore any type of zero-axis controller, such as PI or PR, cannot be implemented since a modulation that would produce a controllable ZSV cannot be used. The SVM proposed by the authors in [14] achieves instantaneous elimination of the ZSV applied by the two VSCs by square wave modulating one VSC and having the other working as an active filter in order to compensate for the distortion introduced by the first one and it is here experimentally validated. In addition the DT effect on the ZSV is considered and the analysis of its effect in conjunction with the modulation proposed is carried out. The square wave modulation allows for easy implementation of instantaneous elimination of the ZSV and allows to use different technologies for the two VSCs. Part I focuses on the analysis of the proposed modulation for instantaneous elimination of the ZSV produced by the dual-inverter. In Part II a novel strategy based on the VSCs' DT to eliminate the sinusoidal ZSC flowing due to the machine's back-EMF and achieve a satisfying phase current waveform is proposed based on the modulation presented in this paper.

II. OEW-PMSM MATHEMATICAL MODEL

The considered electrical system is a 3-phase, p-pole, PMSM [21] where the neutral point of the stator windings has been opened. The stator windings are identical sinusoidally distributed windings, displaced of $120°$ with resistance R_s. The magnetic axes of the stator windings are denoted by the as, bs and cs axes. The machine voltage and flux equations in the abc reference frame are reported in matrix form in (4)

$$\begin{cases} \overline{V}_{PMSM} = RI_{abc} + \dot{\lambda}_{abc} \\ \lambda_{abc} = L_{abc}I_{abc} + \Lambda_r \\ \Lambda_r = \Lambda_{1r} + \Lambda_{3r} \end{cases} \tag{4}$$

where the stator phase voltages $\overline{V}_{PMSM}$ can be written as

$$\overline{V}_{PMSM} = \overline{V}_A - \overline{V}_B = \begin{bmatrix} V_{aa'} \\ V_{bb'} \\ V_{cc'} \end{bmatrix} \tag{5}$$

where $\overline{V}_A$ and $\overline{V}_B$ are the output voltages of the top an lower converter respectively. $V_{aa'}, V_{bb'}$ and $V_{cc'}$ are the OEW-PMSM phase voltages. I_{abc} and λ_{abc} are the phase currents and stator fluxes respectively. The rotor's permanent magnets flux linkage with the stator windings Λ_r has been split in its fundamental Λ_{1r} and third harmonic component Λ_{3r}. Since a common dc-link topology has been chosen the zero-sequence circuit cannot be neglected, therefore the third harmonic back EMF has to be considered. R is a diagonal matrix with R_s on the diagonal, L_{abc}, Λ_{1r} and Λ_{3r} are reported in (1), (2) and (3) respectively. λ_m is the peak flux linkage established by the rotor permanent magnets. $k_{3\lambda}$ is defined as the ratio between the third harmonic flux and λ_m. θ is the rotor angular position of the machine measured as the displacement of the quadrature axis (q) from the magnetic axis of phase as. The direct axis (d) is lagging of $90°$ behind the q axis. Transforming the machine phase voltages equations (1) on the rotor synchronous reference frame the following system is obtained:

$$\begin{bmatrix} V_q^{PMSM} \\ V_d^{PMSM} \\ V_0^{PMSM} \end{bmatrix} = \begin{bmatrix} V_q^A - V_q^B \\ V_d^A - V_d^B \\ V_0^A - V_0^B \end{bmatrix} =$$

$$\begin{bmatrix} R_s & \omega_e L_d & 0 \\ -\omega_e L_q & R_s & 0 \\ 0 & 0 & R_s \end{bmatrix} \begin{bmatrix} i_q \\ i_d \\ i_0 \end{bmatrix} + \tag{6}$$

$$L_{qd0} \frac{d}{dt} \begin{bmatrix} i_q \\ i_d \\ i_0 \end{bmatrix} + \begin{bmatrix} \omega_e \lambda_m \\ 0 \\ 3\omega_e \lambda_m k_{3\lambda} cos(3\theta) \end{bmatrix}$$

where

$$i_0 = \frac{i_a + i_b + i_c}{3} \tag{7}$$

$$L_{abc} = \begin{bmatrix} L_{ls} + L_A - L_B cos(2\theta) & -\frac{1}{2}L_A - L_B cos2(\theta - \frac{\pi}{3}) & -\frac{1}{2}L_A - L_B cos2(\theta + \frac{\pi}{3}) \\ -\frac{1}{2}L_A - L_B cos2(\theta - \frac{\pi}{3}) & L_{ls} + L_A - L_B cos2(\theta - \frac{2\pi}{3}) & -\frac{1}{2}L_A - L_B cos2(\theta + \pi) \\ -\frac{1}{2}L_A - L_B cos2(\theta + \frac{\pi}{3}) & -\frac{1}{2}L_A - L_B cos2(\theta + \pi) & L_{ls} + L_A - L_B cos2(\theta + \frac{2\pi}{3}) \end{bmatrix} \tag{1}$$

$$\Lambda_{1r} = \lambda_m \begin{bmatrix} sin(\theta) & sin(\theta - \frac{\pi}{3}) & sin(\theta + \frac{\pi}{3}) \end{bmatrix}^T \tag{2}$$

$$\Lambda_{3r} = \lambda_m k_{3\lambda} \begin{bmatrix} sin(3\theta) & sin(3\theta) & sin(3\theta) \end{bmatrix}^T \tag{3}$$

Fig. 2. Zero-sequence equivalent circuit. Orange box: VSCs ZSVs; Blue box: OEW-PMSM back EMF.
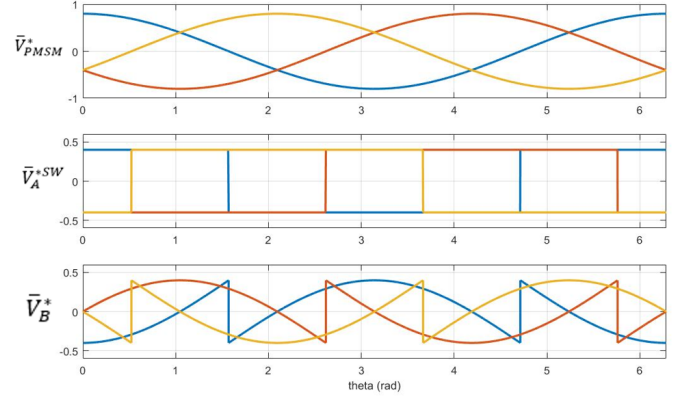

Fig. 3. Reference Voltages for the Dual-Fed OEW-PMSM Drive. Top: FOC output reference voltages. Middle: Square Wave reference voltages for VSC A. Bottom: Reference voltages for the VSC B.

$$L_{qd0} = \begin{bmatrix} L_q & 0 & 0 \\ 0 & L_d & 0 \\ 0 & 0 & L_0 \end{bmatrix} \tag{8}$$

ω_e is the machine electrical speed, L_q, L_d and L_0 are the q, d and 0 axes inductances respectively. The relationship between L_A, L_B, L_{ls} and the machine's inductances L_q, L_d and L_0 in the synchronous reference frame is reported in (9). The sum of the phase currents is no longer zero since a common dc-link DF OEW-PMSM topology has been chosen, therefore a ZSC i_0 is free to flow in the system.

$$L_q = \frac{3(L_A - L_B)}{2}; \ L_d = \frac{3(L_A + L_B)}{2}; \ L_l s = L_0 \tag{9}$$

A. Zero Sequence Equivalent Circuit

Whether the ZSC magnitude is acceptable it depends on the machine parameters (R_s, L_0 and zero sequence back EMF) which could lead to high magnitude current ripple that could potentially harm the switching devices. The equivalent circuit of the zero-sequence axes can be derived from the third line of (6) and it is shown in Fig. 2, where V_0^A and V_0^B are generated by the VSCs and $3\omega_e\lambda_m k_{3\lambda}\cos(3\theta)$ is generated by the third harmonic back EMF. The harmonic content of the machine flux often contains the third harmonic component therefore even if the VSCs' ZSV $V_0^A - V_0^B$ would be cancelled the ZSC would still flow due to the third harmonic back EMF.

III. REFERENCE VOLTAGE GENERATION FOR THE DUAL-FED OEW-PMSM DRIVE

The duty cycles for the two VSCs are generated with the intention to keep instantaneously at zero the V_0^{PMSM} and to exploit the different nature of the two technologies used, IGBT and SiC devices. The voltage on the OEW-PMSM can be expressed as the difference between the VSC A voltage and the B one (4). The same relationship is used to generate the reference voltages for the two VSCs.

$$\overline{V}_{PMSM}^* = \overline{V}_A^* - \overline{V}_B^* \tag{10}$$

Where $\overline{V}_{PMSM}^*$ are the OEW-PMSM reference phase voltages, $\overline{V}_A^*$ and $\overline{V}_B^*$ are respectively the reference phase voltages of the A and B VSCs. The OEW-PMSM reference voltages $\overline{V}_{PMSM}^*$ are obtained from a standard Field Oriented Control (FOC) and then used to obtain the reference signals for the A VSC as follows

$$\overline{V}_A^{*SW} = \frac{V_{dc}}{2} sign(\overline{V}_{PMSM}^*) \tag{11}$$

(11) shows that the A VSC reference voltages consist in three square-wave voltages of amplitude $\frac{V_{dc}}{2}$ with the same phase displacement of the OEW-PMSM reference voltage signals. The reference signals for the B VSC are obtained from (10) substituting $\overline{V}_A^{*SW}$ to $\overline{V}_A^*$

$$\overline{V}_B^* = \overline{V}_A^{*SW} - \overline{V}_{PMSM}^* \tag{12}$$

The reference voltages split for the two VSCs as described in (10)-(12) consist of a square wave control of the IGBT converter allowing it to switch at the fundamental frequency set by the motor speed. By setting the VSC A to modulate in square-wave mode a simple and known profile for the converter's voltages is set. Therefore the same profile of V_0^A can be instantaneously synthesized by the VSC B in order to have $V_0^A - V_0^B$ equal to zero. Fig. 3 shows the profiles of the normalised reference voltages over an electrical period. A SVM modulation that allows to satisfy at each sample time the conditions set by (12) and V_0^{PMSM} equal to zero has been developed and presented in Section IV. The six-step modulation of VSC A introduces elevated harmonic distortion therefore VSC B needs to switch at an higher frequency in order to compensate for it. Different technologies can be used for the two VSCs. The slow switching VSC A can be realised with IGBT devices while VSC B with SiC ones. The role of the SiC converter in this configuration can be interpreted as an active filter that eliminates the harmonic distortion introduced by the low switching IGBT one simultaneously providing the high switching frequency necessary to synthesize the fundamental of the machine. This separation of the reference signals $\overline{V}_{PMSM}^*$ between the two VSCs results in an increased efficiency of the overall architecture and allows exploitation of the different natures of the two converters [10], [11]. Considering the different switching frequencies of the two converters the IGBT is mainly responsible for the conduction

losses while the SiC is responsible for the switching losses. E.g. if we consider a 3 pole pairs OEW-PMSM rotating at 3000 rpm the IGBT converter switching frequency would be 150 Hz.

IV. OEW-PMSM MODULATION STRATEGY FOR INSTANTANEOUS ZSV ELIMINATION

A. Dual Inverter Voltage Vectors

From Fig. 1 the phase voltages of the OEW-PMSM as a function of the switching states can be written as:

$$\begin{bmatrix} V_{aa'} \\ V_{bb'} \\ V_{cc'} \end{bmatrix} = \begin{bmatrix} s_a^1 - s_a^2 \\ s_b^1 - s_b^2 \\ s_c^1 - s_c^2 \end{bmatrix} V_{dc} \qquad (13)$$

Where s_k^h indicates the switching state of the inverter leg and it can be equal to 1 if the switch device on the upper bridge turns on or 0 if the switch device turns off. It is therefore possible to identify the state of the inverter leg exclusively by the state of the upper switch. Subscript k indicates the phase while superscript h stands for the VSC A when equal to 1 or the VSC B when equal to 2. In the stationary $\alpha\beta0$ coordinate frame the VSCs phase voltages of (6) can be transformed on the stationary reference frame as (14).

$$\begin{bmatrix} V_\alpha \\ V_\beta \\ V_0 \end{bmatrix} = \frac{2}{3} \begin{bmatrix} 1 & -\frac{1}{2} & -\frac{1}{2} \\ 0 & \frac{\sqrt{3}}{2} & -\frac{\sqrt{3}}{2} \\ \frac{1}{2} & \frac{1}{2} & \frac{1}{2} \end{bmatrix} \begin{bmatrix} V_{aa'} \\ V_{bb'} \\ V_{cc'} \end{bmatrix} \qquad (14)$$

It follows that there are $2^6 = 64$ possible combinations of switching states: they are the possible realisations of 19 different space voltage vectors of which 18 are active vectors corresponding to the vertices of the black, blue and red hexagons of Fig. 4, and 1 zero vector located at the origin. It should be noted that this configuration provides a number of different space voltage vectors equal to the one of a three-level inverter. However, if the VSCs ZSV $V_0^A - V_0^B$ wants to be kept to zero to avoid ZSC circulation, all the vectors that generate a non-zero V_0 cannot be used. The admissible switching states that can be used to synthesize the voltage control actions are the ones with zero V_0 component. The 64 switching states reduce to 20: they can produce 1 zero vector at the origin and 6 different active vectors corresponding to the vertexes of the red hexagon of Fig. 4.

The modulation index m is defined as

$$m = \frac{|\bar{V}|^*}{V_{dc}} \qquad (15)$$

Where $\bar{V}^*$ is the reference voltage vector. Always referring to Fig. 4 the maximum modulation indexes are $\frac{1}{\sqrt{3}}$, 1 and $\frac{2}{\sqrt{3}}$ for the black hexagon, the red one and the blue one respectively. Working with space vectors with no ZSV corresponds to work on the red hexagon thus having a reduction of 13.4% compared to the maximum modulation index that this double converter configuration would allow. The dc-link utilisation is still higher if compared with a standard single VSI drive gaining 42.3%.
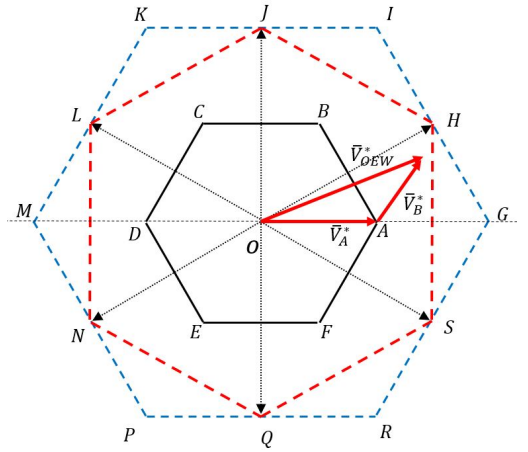

Fig. 4. Space Voltage Vectors for the dual Inverter. Single VSC voltage vectors (Black hexagon), Dual Inverter voltage vectors (blue dotted hexagon) and dual inverter voltage vectors with zero V_0^{PMSM} (red dashed hexagon)
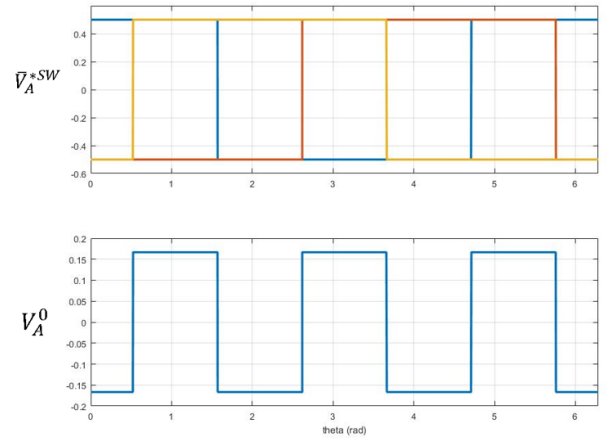

Fig. 5. ZSV for the single three phase VSC drive when modulated in six-step. Top: Normalised phase voltages of the square wave modulated VSC. Bottom: normalised ZSV V_0^A.

B. SVM for Instantaneous ZSV Elimination

In order to have zero V_0^{PMSM} applied on the machine the ZSVs produced by the two VSCs V_0^A and V_0^B must be instantaneously the same. An efficient solution to achieve zero V_0^{PMSM} is to choose a particular modulation for one of the two VSCs so that the ZSV can be easily described as a function of the converter reference voltage angle. I.e. if the VSC A is modulated in six-step mode its ZSV V_0^A has a well known profile. Fig. 5 shows the ZSV profile of a single VSC which is modulated in square wave mode. Table I shows the voltage components in the $\alpha\beta0$ reference system for the 8 switching states for a single VSC. Operating in square wave a VSC means applying only the 6 active vectors and jumping from one to the adjacent according to the verse of rotation of the machine. According to Table I the ZSV of the square wave modulated VSC V_0^A corresponds to a square wave that assumes the values $\pm\frac{1}{6}V_{dc}$ with period $\frac{2\pi}{3\omega_e}$. By adopting a conventional triangular wave PWM for the B converter the resulting V_0^{PMSM} on the OEW-PMSM would

not be instantaneously equal to 0. In fact all the possible voltage state corresponding to the blue hexagon of Fig. 4 are used. A modulation for the B VSC is developed in order to instantaneously set V_0^B equal to V_0^A. The active vectors of the single inverter can be grouped in two sets, the ones that produce a negative ZSV (V_A, V_C and V_E) and the ones that produce a positive ZSV (V_B, V_D and V_F). According to which set belongs the active voltage vector that the square-wave modulated VSC A is applying the B one can only apply the three active voltage vectors which have the same ZSV component. The dwelling times for the three active vectors can be found similarly as done for a standard SVM. For the first set of vectors V_A, V_C and V_E the following system can be written

$$\begin{cases} Re(\overline{V}^*_B) = t_{V_A} V - t_{V_C}\dfrac{V}{2} - t_{V_E}\dfrac{V}{2} \\ Im(\overline{V}^*_B) = t_{V_C}\dfrac{\sqrt{3}V}{2} - t_{V_E}\dfrac{\sqrt{3}V}{2} \\ T_s = t_{V_A} + t_{V_C} + t_{V_E} \end{cases} \quad (16)$$

Similarly can be done for the set of vectors V_B, V_D and V_F

$$\begin{cases} Re(\overline{V}^*_B) = t_{V_B}\dfrac{V}{2} - t_{V_D}V + t_{V_F}\dfrac{V}{2} \\ Im(\overline{V}^*_B) = t_{V_B}\dfrac{\sqrt{3}V}{2} - t_{V_F}\dfrac{\sqrt{3}V}{2} \\ T_s = t_{V_B} + t_{V_D} + t_{V_F} \end{cases} \quad (17)$$

Where V is the module of the VSC's vectors in the $\alpha\beta$ plane that correspond to $\frac{2V_{dc}}{3}$ and T_s is the system sample time. By solving the system of equations (16) and (17) for $t_{V_A}, t_{V_C}, t_{V_E}$ and $t_{V_B}, t_{V_D}, t_{V_F}$ respectively the dwelling times for the voltage vectors of the VSC B can be found. At each T_s the square wave reference voltages are calculated according to (11), then it is checked if the reference voltage vector $\overline{V}^{*SW}_A$ belongs to the set of vectors that produce a positive or negative ZSV. According to which set it belongs either (16) or (17) are used to calculate the dwelling times for the voltage vectors of the B VSC. The three active voltage vectors are applied in ascending order from the one which has the shortest dwelling time to the longest. The three vectors can therefore be applied in 3! = 6 possible permutations. The three vectors will be identified as t_{min}, t_{med} and t_{max} according to their dwelling time. Thanks to the modulation introduced the ZSV V_0^{PMSM} generated by the converters is instantaneously zero apart from the voltage distortion introduced by the DTs, therefore a ZSC PI controller is not needed. The elimination of the ZSV produced by the dual-inverter thanks to the proposed modulation can be achieved all over the operating points that fall inside the red hexagon of Fig. 4 and it is independent from the system parameters.

V. DEAD-TIME EFFECT ON OEW-PMSM ZSV

Failure of the switching devices and even of the whole inverter is possible if a DT is not added in the control scheme to ensure proper operation of the inverter. In this way the bridge shoot through can always be avoided eliminating additional losses or even thermal runaway. Usually several micro seconds are required for the DT which are no longer

TABLE I
SINGLE INVERTER SWITCHING STATES

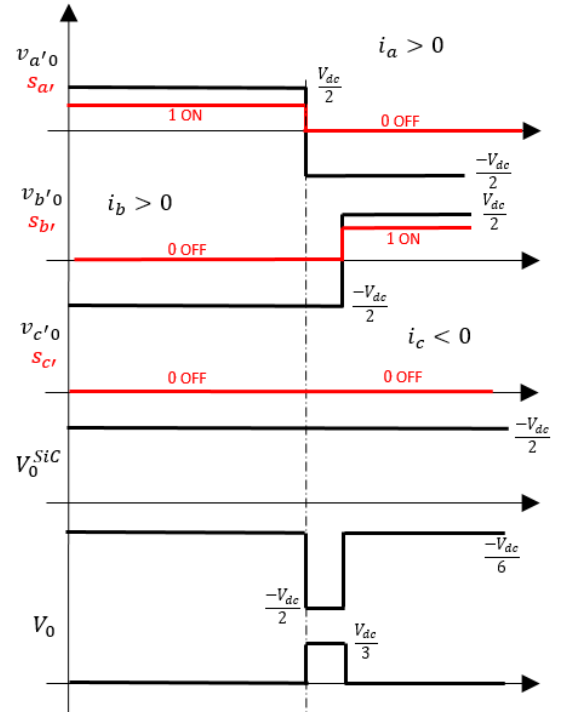| Voltage Vector	Gate Signals	V_α	V_β	V_0
V_0	[0 0 0]	0	0	$-1/2$
V_A	[1 0 0]	$2/3$	0	$-1/6$
V_B	[1 1 0]	$1/3$	$1/\sqrt{3}$	$1/6$
V_C	[0 1 0]	$-1/3$	$1/\sqrt{3}$	$-1/6$
V_D	[0 1 1]	$-2/3$	0	$1/6$
V_E	[0 0 1]	$-1/3$	$-1/\sqrt{3}$	$-1/6$
V_F	[1 0 1]	$1/3$	$-1/\sqrt{3}$	$1/6$
V_7	[1 1 1]	0	0	$1/2$

Fig. 6. DT effect on V_0^{PMSM}. Gate signals in red, voltages in black. From top: top gate signal of leg a of VSC B and relative voltage. top gate signal of leg b of VSC B and relative voltage. top gate signal of leg c of VSC B and relative voltage. ZSV V_0^B of VSC B and ZSV V_0^{PMSM} on the OEW-PMSM

ignorable in the inverter modelling. Even if the gate signal DT is always applied, the phase voltage distortion happens only in the two following cases: s_j switches from 0 to 1 and $i_j > 0$ or s_j switches from 1 to 0 and $i_j < 0$ where i is the phase current, s is the switching state of the leg top device and j stands for the jth inverter leg. Fig. 6 shows the three states of VSC B and their output phase voltages $v_{a'0}, v_{b'0}$ and $v_{c'0}$ in the case of $i_a > 0, i_b > 0$ and $i_c < 0$. The set of vectors which produce a negative ZSV is considered, in particular the transition from V_A to V_C is analysed. Therefore the DT will cause a voltage distortion only on $v_{b'0}$. In fact when both the upper and lower devices are off the phase current will keep flowing through the lower diode keeping the voltage clamped to $-\frac{V_{dc}}{2}$. During the DT the ZSV V_0^A is $-\frac{V_{dc}}{2}$ different from the ZSV produced by VSC A which is $-\frac{V_{dc}}{6}$. The result is a positive ZSV V_0 of $\frac{V_{dc}}{3}$ on the machine that will cause a ZSC to circulate. It can be noticed that for the same switching V_A to V_C with $i_a < 0, i_b < 0$ and $i_c > 0$ that the DT distortion

L_q	355 [μH]	L_d	355 [μH]
R_s	1.64 [$m\Omega$]	p	3 [-]
λ_m	0.086532 [V s]	$k_{3\lambda}$	$1.41 10^{-3}$ [-]

Fig. 7. Simulation Results. 8000 rpm, standard PWM. Top: phase current i_a; Middle: ZSC; Bottom: ZSV.
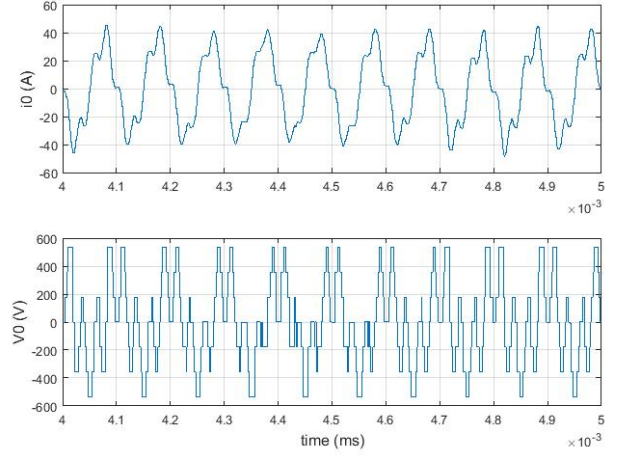

Fig. 8. Simulation Results, detail of ZSC and ZSV. 8000 rpm, standard PWM. Top: ZSC; Bottom: ZSV.
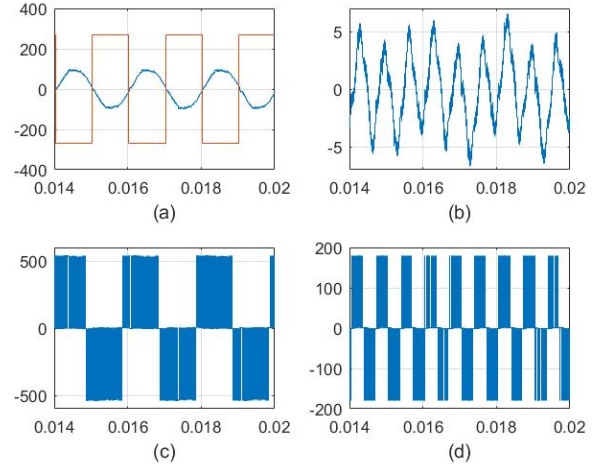

Fig. 9. Simulation Results for the proposed SVPWM for istantaneous ZSV elimination. 10000 rpm. (a) Phase current i_a. X-axis: 2ms/div; Y-axis: 200 A/div; V_{a0} (red line) X-axis: 2ms/div; Y-axis: 200 V/div.(b) ZSC i_0. X-axis: 2ms/div; Y-axis: 5 A/div (c) Phase voltage Vaa'. X-axis: 2ms/div; Y-axis: 500 V/div (d) ZSV V_0^{PMSM}. X-axis: 2ms/div; Y-axis: 100 V/div

on leg a' due to a transition from 1 to 0 causes a negative ZSV of $-\frac{V_{dc}}{3}$ on the machine. Similarly the same analysis can be done for the set of vectors $t_{V_B}, t_{V_D}, t_{V_F}$ which produce a positive ZSV observing the same behaviour as the vectors $t_{V_A}, t_{V_C}, t_{V_E}$.

VI. SIMULATIONS RESULTS

Simulations of the proposed method have been analysed in Matlab-Simulink. The high speed starter-generator OEW-PMSM parameters are reported in Table II. The dc-link voltage is set to 540 V with the IGBT and SiC VSCs switching frequencies of 10 and 40 KHz respectively. The q and d axis current control is achieved by two simple PI regulators with gains selected in order to have an equivalent bandwidth of 1 KHz. The performances of the proposed topology when a standard PWM is used for both the converters are shown in Fig. 7. A common way to obtain the reference voltages for the two VSCs is to split the voltage reference into two vectors of same length but opposite phase. Therefore $\overline{V}_A^*$ and $\overline{V}_B^*$ correspond to $\frac{\overline{V}_{PMSM}^*}{2}$ and $-\frac{\overline{V}_{PMSM}^*}{2}$ respectively as done in [17]. It can be noticed the high intensity ZSC ripple due to the ZSV applied by the VSCs which is superimposed to the third harmonic oscillation. A detail of the ZSC ripple and the ZSV are shown in Fig. 8, the ZSV is different from zero and it reaches peaks of V_{dc}. In Fig. 9 the performances when the proposed SVPWM for instantaneous ZSV elimination are presented. Thanks to the modulation introduced the ZSV corresponds only to the distortion of $\pm\frac{V_{dc}}{3}$ introduced by the DT.

VII. EXPERIMENTAL RESULTS

The proposed topology performances have been tested on an experimental set-up composed by an OEW-PMSM coupled with a DC motor as shown in Fig. 10. The recursive least square method [22] has been used to estimate both the electrical and mechanical parameters of the motor. The parameters of the OEW-PMSM used for experimental validation are reported in Table III. Even though the high speed machine of which previously discussed was still not available, the used set-up still shows the same problems on a smaller scale. The machine used is a 1.5 KW PMSM with a rated speed of 3000 rpm therefore characterized by much lower rated current than the high speed starter-generator. The low ZSI still causes high distortion on the machine phase currents, therefore it can be used effectively to experimentally validate the presented work. The control board specification can be found in [23]. The dc-

TABLE III
OEW-PMSM under test Parameters

L_q	1.2 [mH]	L_d	1.2 [mH]
R_s	0.99 [Ω]	p	3 [-]
λ_m	0.0286 [V s]	$k_{3\lambda}$	3.7510^{-4} [rpm]

link voltage is 80 V, the IGBT VSC is switched in square wave mode while the SiC VSC switching frequency is 40 KHz. The IGBT DT is set to $3\mu s$ while the SiC one to $1\mu s$. Since the modulation proposed for the ZSV elimination is independent from the operating point of the machine, exclusively the inertial load case and a few operating speeds have been considered. Similarly as done in Fig. 7 the performances of the proposed system when two standard PWM are used for both converters are checked. Fig. 11 shows the distortion introduced by the ZSC on the phase current profile. Both the third harmonic back EMF component and the switching ZSV contribute can be identified on the ZSC. In fact the ZSC has a period that is three times the phase current and shows a high frequency intense ripple due to the fact that a standard PWM that allows to move on the whole blue hexagon of Fig. 4 is used. A detail of the ZSC and ZSV of Fig. 11 is reported in Fig. 12 showing a behaviour very similar to simulation results presented in Fig. 8. Fig. 13 shows the implementation of the proposed modulation. The VSC A, i.e. the IGBT one is square wave modulated while the VSC B, i.e. the SiC one is modulated according to (12) with a switching frequency of 40 KHz. The IGBT converter now switches at the machine fundamental frequency as it can be seen from Fig. 13 (a) where the phase current and the IGBT phase voltage are shown. The third harmonic component superimposed to the phase current due to the non-sinusoidal back EMF is still present. It can be noticed how the ZSV applied to the machine goes from 20 to -20 V which correspond to the voltage distortion introduced by the DT. Fig. 14 shows the experimental results obtained running the machine at 1600 rpm but applying a load torque instead of having only the inertial one. The higher waveform quality can be associated with the increased torque applied by the OEW-PMSM. ZSC is still present due to the third harmonic back-EMF of the machine therefore significantly reducing the phase current waveform quality. In Part II of this paper a novel DT Hysteresis control of the ZSC is discussed to eliminate the circulation of additional currents due to the non-sinusoidal machine back-EMF.

VIII. Conclusions

In this paper a dual-fed common dc link topology OEW-PMSM for aircraft high speed Starter-Generator application is considered. A novel hybrid SVPWM has been developed for the dual VSC in order to instantaneously eliminate the ZSV produced by the VSCs. The OEW-PMSM model has been presented considering the non-sinusoidal machine back EMF, furthermore analysis of the effect of the VSCs' DT on the ZSV has been carried out. Considering the new modulation proposed where one of the VSCs works in square wave mode, mixed technology is used for the two VSCs in order to obtain higher system efficiency and reduce the ZSC circulating
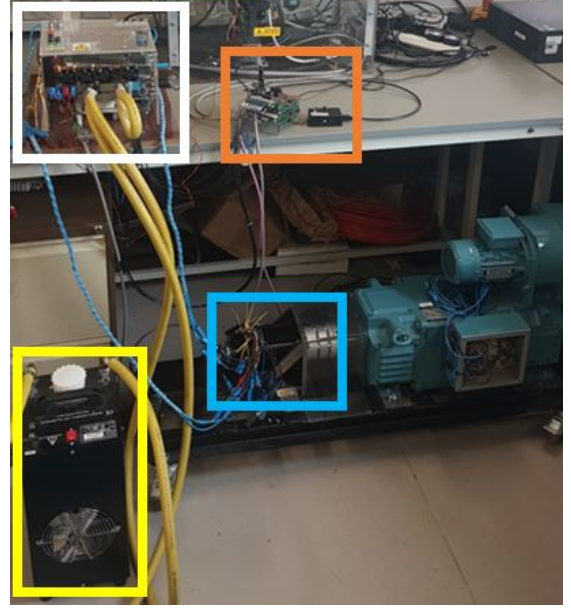

Fig. 10. Experimental set-up: Mixed technology IGBT-SiC common dc link conerter (white rectangle), control board (orange rectangle), chiller for liquid cooling of VSCs (yellow rectangle) and OEW-PMSM (blue rectangle).
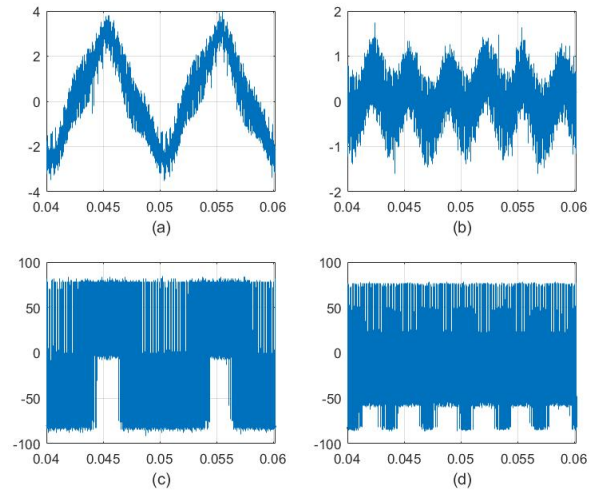

Fig. 11. Speed wm of 2000 rpm. Standard PWM. (a) Phase current i_a. X-axis: 5ms/div; Y-axis: 2 A/div (b) ZSC i_0. X-axis: 5ms/div; Y-axis: 1 A/div (c) Phase voltage Vaa'. X-axis: 5ms/div; Y-axis: 50 V/div (d) ZSV V_0^{PMSM}. X-axis: 5ms/div; Y-axis: 50 V/div

problem. The proposed techniques have been tested through simulations and verified experimentally.

References

[1] H. Stemmler and P. Guggenbach, "Configurations of high-power voltage source inverter drives," in *1993 Fifth European Conference on Power Electronics and Applications*, Sept 1993, pp. 7–14 vol.5.

[2] T. M. Jahns, "Improved reliability in solid-state ac drives by means of multiple independent phase drive units," *IEEE Transactions on Industry Applications*, vol. IA-16, no. 3, pp. 321–331, May 1980.

[3] B. C. Mecrow, A. G. Jack, J. A. Haylock, and J. Coles, "Fault-tolerant permanent magnet machine drives," *IEE Proceedings - Electric Power Applications*, vol. 143, no. 6, pp. 437–442, Nov 1996.
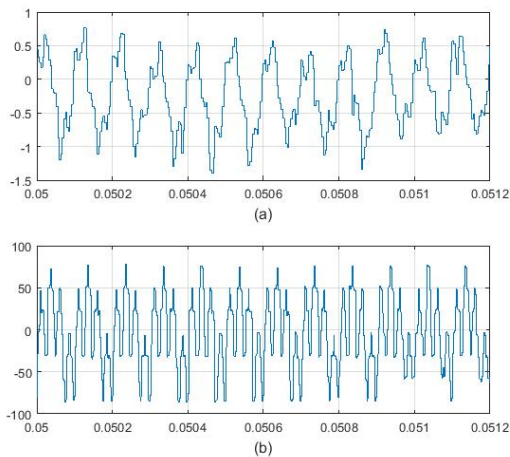
Fig. 14. Experimental results at wm of 1600 rpm and increased load torque. Top: Phase current i_a, i_b, i_c (blue, red, and yellow respectively). Bottom: ZSC i_0.

Fig. 12. Speed wm of 2000 rpm. Standard PWM. (a) ZSC i_0. X-axis: 0.2ms/div; Y-axis: 0.5 A/div (b) ZSV V_0^{PMSM}. X-axis: 0.2ms/div; Y-axis: 50 V/div
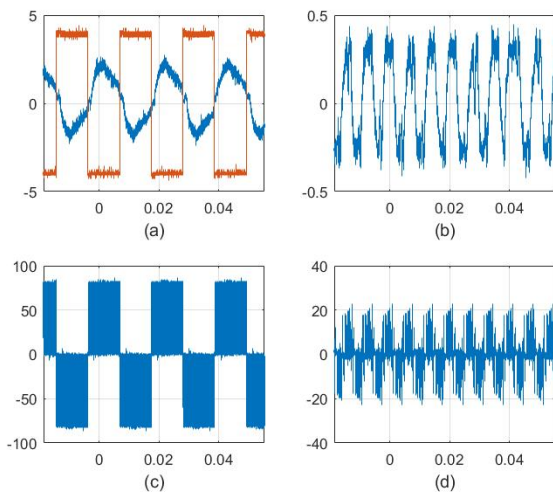

Fig. 13. Speed wm of 1000 rpm. Proposed modulation. (a) Phase current i_a (blue line) X-axis: 5ms/div; Y-axis: 5 A/div, V_{a0} (red line) X-axis: 5ms/div; Y-axis: 100 V/div. X-axis: 5ms/div; Y-axis: 5 A/div (b) ZSC i_0. X-axis: 5ms/div; Y-axis: 0.5 A/div (c) Phase voltage Vaa'. X-axis: 5ms/div; Y-axis: 50 V/div (d) ZSV V_0^{PMSM}. X-axis: 5ms/div; Y-axis: 20 V/div

[4] Y. Zhou and H. Nian, "Zero-sequence current suppression strategy of open-winding pmsg system with common dc bus based on zero vector redistribution," *IEEE Transactions on Industrial Electronics*, vol. 62, no. 6, pp. 3399–3408, June 2015.

[5] Y. Wang, D. Panda, T. A. Lipo, and D. Pan, "Pulsewidth-modulated dual-half-controlled converter," *IEEE Transactions on Power Electronics*, vol. 28, no. 2, pp. 959–969, Feb 2013.

[6] B. A. Welchko and J. M. Nagashima, "The influence of topology selection on the design of ev/hev propulsion systems," *IEEE Power Electronics Letters*, vol. 1, no. 2, pp. 36–40, June 2003.

[7] J. Kim, J. Jung, and K. Nam, "Dual-inverter control strategy for high-speed operation of ev induction motors," *IEEE Transactions on Industrial Electronics*, vol. 51, no. 2, pp. 312–320, April 2004.

[8] A. P. Sandulescu, F. Meinguet, X. Kestelyn, E. Semail, and A. Bruyere, "Flux-weakening operation of open-end winding drive integrating a cost-effective high-power charger," *IET Electrical Systems in Transportation*, vol. 3, no. 1, pp. 10–21, March 2013.

[9] J. Wei, Q. Deng, B. Zhou, M. Shi, and Y. Liu, "The control strategy of open-winding permanent magnet starter-generator with inverter-rectifier topology," *IEEE Transactions on Industrial Informatics*, vol. 9, no. 2,
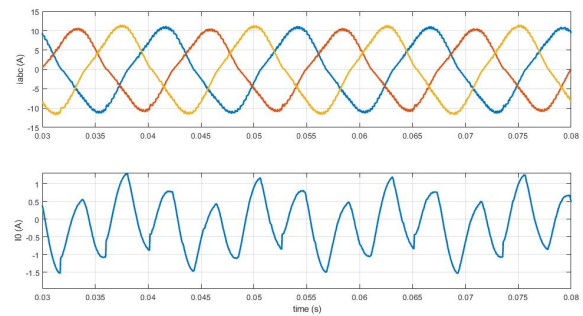
pp. 983–991, May 2013.

[10] G. L. Calzo, P. Zanchetta, C. Gerada, A. Gaeta, and F. Crescim-bini, "Converter topologies comparison for more electric aircrafts high speed starter/generator application," in *2015 IEEE Energy Conversion Congress and Exposition (ECCE)*, Sept 2015, pp. 3659–3666.

[11] G. L. Calzo, P. Zanchetta, C. Gerada, A. Lidozzi, M. Degano, F. Crescimbini, and L. Solero, "Performance evaluation of converter topologies for high speed starter/generator in aircraft applications," in *IECON 2014 - 40th Annual Conference of the IEEE Industrial Electronics Society*, Oct 2014, pp. 1707–1712.

[12] D. Casadei, G. Grandi, A. Lega, C. Rossi, and L. Zarri, "Switching technique for dual-two level inverter supplied by two separate sources," in *APEC 07 - Twenty-Second Annual IEEE Applied Power Electronics Conference and Exposition*, Feb 2007, pp. 1522–1528.

[13] M. Mengoni, A. Amerise, L. Zarri, A. Tani, G. Serra, and D. Casadei, "Control scheme for open-ended induction motor drives with a floating capacitor bridge over a wide speed range," *IEEE Transactions on Industry Applications*, vol. 53, no. 5, pp. 4504–4514, Sept 2017.

[14] L. Rovere, A. Formentini, G. L. Calzo, P. Zanchetta, and T. Cox, "Igbt-sic dual fed open end winding pmsm drive," in *2017 IEEE International Electric Machines and Drives Conference (IEMDC)*, May 2017, pp. 1–7.

[15] A. Somani, R. K. Gupta, K. K. Mohapatra, and N. Mohan, "On the causes of circulating currents in pwm drives with open-end winding ac machines," *IEEE Transactions on Industrial Electronics*, vol. 60, no. 9, pp. 3670–3678, Sept 2013.

[16] H. Zhan, Z. Zhu, and M. Odavic, "Analysis and suppression of zero sequence circulating current in open winding pmsm drives with common dc bus," *IEEE Transactions on Industry Applications*, vol. 53, no. 4, pp. 3609–3620, July 2017.

[17] V. T. Somasekhar, S. Srinivas, and K. K. Kumar, "Effect of zero-vector placement in a dual-inverter fed open-end winding induction-motor drive with a decoupled space-vector pwm strategy," *IEEE Transactions on Industrial Electronics*, vol. 55, no. 6, pp. 2497–2505, June 2008.

[18] P. Sandulescu, F. Meinguet, X. Kestelyn, E. Semail, and A. Bruyre, "Control strategies for open-end winding drives operating in the flux-weakening region," *IEEE Transactions on Power Electronics*, vol. 29, no. 9, pp. 4829–4842, Sept 2014.

[19] Q. An, J. Liu, Z. Peng, L. Sun, and L. Sun, "Dual-space vector control of open-end winding permanent magnet synchronous motor drive fed by dual inverter," *IEEE Transactions on Power Electronics*, vol. 31, no. 12, pp. 8329–8342, Dec 2016.

[20] H. Zhan, Z. Q. Zhu, M. Odavic, and Y. Li, "A novel zero-sequence model-based sensorless method for open-winding pmsm with common dc bus," *IEEE Transactions on Industrial Electronics*, vol. 63, no. 11, pp. 6777–6789, Nov 2016.

[21] S. D. S. Paul C. Krause, Oleg Wasynczuk, in *Analysis of electric machinery and drive systems 2nd ed.* New York IEEE Press - IEEE Press power engineering series, 2002, pp. 191–206.

[22] T. Soderstrom and P. Stoica, in *System Identification.* Prentice Hall International Series in Systems and Control Engineering, 1994, pp. 320–324.

[23] A. Galassini, G. L. Calzo, A. Formentini, C. Gerada, P. Zanchetta, and A. Costabeber, "ucube: Control platform for power electronics," in *2017 IEEE Workshop on Electrical Machines Design, Control and Diagnosis (WEMDCD)*, April 2017, pp. 216–221.